

SATURN ELECTROSTATIC DISCHARGES CHARACTERISTICS, COMPARISON TO PLANETARY LIGHTNING AND IMPORTANCE IN THE STUDY OF SATURN'S IONOSPHERE

P. Zarka*

Abstract

The characteristics of Saturn electrostatic discharges (SED) observed by the two Voyager Planetary Radio Astronomy experiments are exhaustively reviewed: appearance, duration, spectrum, polarization, intensity and periodicity of occurrence. Their study allowed to localize the emission source in Saturn's equatorial atmosphere, and to determine its size and beaming pattern. The comparison of their characteristics with the properties of other planetary lightning led to identify SED as the radio emission associated to Saturnian lightning. Moreover, the use of the SED source as a natural probe of Saturn's ionosphere allowed to derive the diurnal variations of the ionospheric electron density over the equatorial zone of the planet. The future observations of SED-associated phenomena are briefly outlined.

1 Introduction

Five days before its encounter with Saturn in November 1980 the Planetary Radio Astronomy (PRA) experiment on board the Voyager 1 (V1) spacecraft discovered an unexpected but intense non-magnetospheric radio emission. Figure 1 displays the trajectory of V1 around closest approach (which occurred on November 12 (day 317), 1980, at spacecraft time 23:56). This emission was also observed by Voyager 2 (V2) during a few days around its closest approach to Saturn, on August 26 (day 238), 1981, at spacecraft time 3:24.

2 Description of the SED emission

The PRA experiment [Warwick et al., 1977] consists of a pair of 10-m orthogonal monopoles loaded against the conductive structure of the spacecraft, and connected to

*Paris-Meudon Observatory, Laboratoire Associe du CNRS 324, 92195 MEUDON PRINCIPAL CEDEX, FRANCE

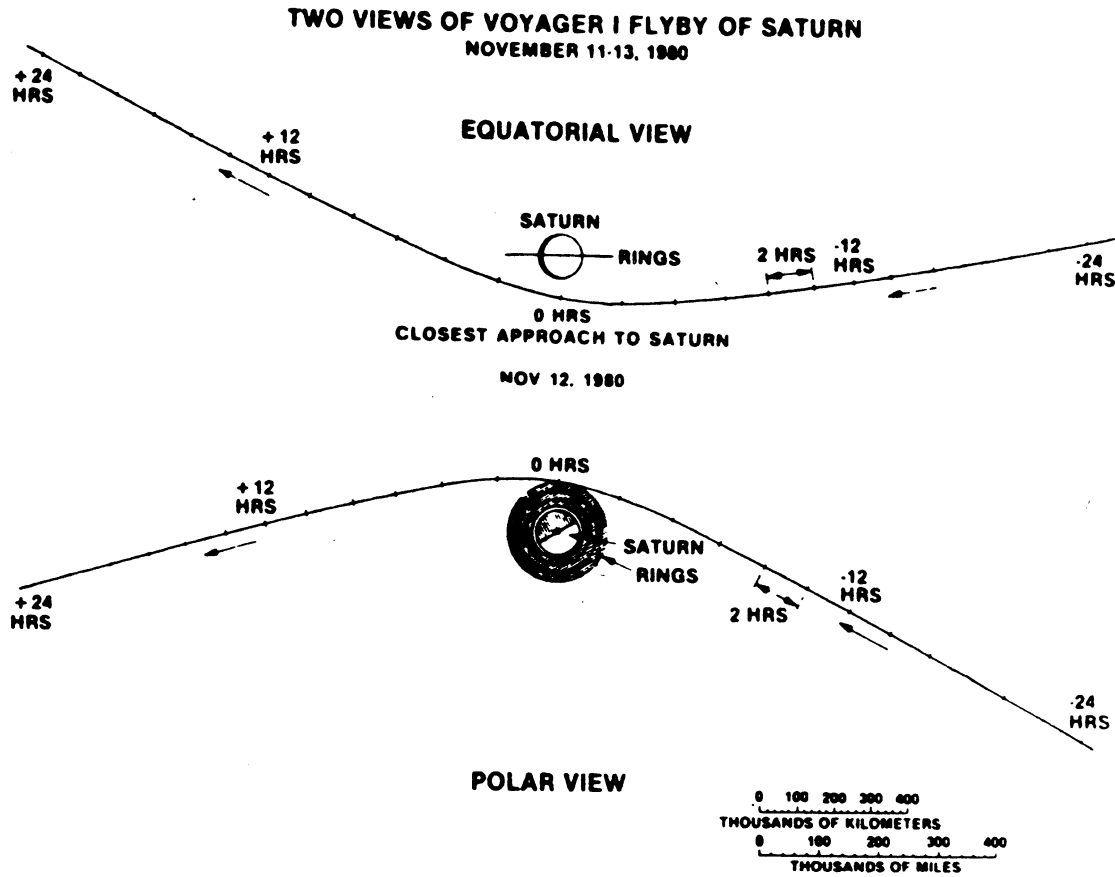


Figure 1: Voyager 1 trajectory around closest approach to Saturn (NASA document).

a high-sensitivity broadband receiver (1.2 kHz to 40.2 MHz). The basic mode of the instrument allows to obtain dynamic spectra of the planetary radio emissions, as the one displayed on Figure 2a. These spectra are created by 6-s 198-step, scans at 30 ms per step, in 128 200-kHz-wide channels uniformly spaced from 40.2 to 1.2 MHz, and 70 1-kHz-wide channels uniformly spaced from 1326 to 1.2 kHz. Each channel measures the detected flux density alternatively in left- and right-hand circular polarization. On the figure Saturn kilometric radiation (SKR) is detected in the frequency range 200–700 kHz.

Saturn electrostatic discharges (SED) are the short streaks parallel to the frequency axis. The fact that they are randomly distributed over the whole frequency range of the PRA receiver has led Warwick et al. [1981] to interpret them as short-duration (30 to \sim 400 ms) broadband (\geq 40 MHz) bursts, recorded only in the channels sampled during their occurrence. These authors also ruled out any sort of interference (spacecraft-generated or due to nearby discharging phenomena) as the source of these bursts, and concluded that Voyager was observing the effects of short-lived electrostatic discharges originating from the vicinity of Saturn and propagating to the spacecraft. Due to their resemblance with the radio signature of terrestrial lightning, as displayed on Figure 2b, these bursts were named “SED” for Saturn Electrostatic Discharges [Warwick et al., 1981].

This resemblance is also evident on Figure 3 where high time-resolution radio measure-

ments of SED and terrestrial lightning are compared. The data displayed on Figure 3a were recorded by the V1 PRA receiver in an alternate operating mode, in which two adjacent channels at 9.5 and 9.8 MHz with orthogonal polarization states are alternatively sampled every 70 μ s. With this time resolution the SED emission appears very impulsive, identical in the two polarization states, and without frequency drift. This confirms the interpretation of SED as impulsive broadband phenomena. Important intensity fluctuations at the time resolution limit of the PRA high-rate mode (140 μ s) led Warwick et al. [1981] to estimate an upper limit of about 40 km for the size of the instantaneous radio source.

3 Statistical results

3.1 Duration, Occurrence

SED have a duration of 30 to \sim 400 ms with a mean value of 57 ms near closest approach [Zarka and Pedersen, 1983]. The distributions of SED durations for the V1 and V2 encounter periods, displayed on Figure 4, are very well described by the same exponential law in $N = N_0 e^{D/D_0}$ (where N is the number of bursts with a duration D) with an e-folding time $D_0 \sim 45$ ms. However, the absolute occurrence of SED was 3.5 times less in the case of V2. The maximum occurrence rate of SED (i.e. near closest approach) was 1.4% for V1 and 0.4% for V2. This corresponds to an emission rate of 0.25 per second for V1 (and 0.07 per second for V2).

Evans et al. [1983] showed that the distribution of the number of SED per time unit was well described by a Poisson distribution. Warwick et al. [1981] found from the high time resolution data that the fine structure of a SED burst consists of very short elementary bursts (< 1 msec) superimposed on a strong continuum.

3.2 Periodicity of Occurrence

One of the most interesting properties of SED was the grouping of individual events into distinct episodes recurring with a periodicity about 10h 10min [Warwick et al., 1981, 1982; Evans et al., 1981], clearly different from Saturn's rotation period of 10h 39.4min \pm 0.1min.

Figure 5 is a very revealing way of representing the data. On the upper figures (a,b), SED events appearing in the high-frequency band of the PRA receiver have been plotted versus time (with a compressed time scale) and frequency for the main part of each Voyager-Saturn encounter (the low band was often swamped by the SKR which is sporadic too). The corresponding occurrence diagrams are plotted on the lower figures (c,d). On these figures the episode structure as well as the $1/R^2$ decreasing amount of SED (where R is the distance between the spacecraft and the planet) appear clearly. The SED are not only less numerous for V2, but the episodic structure of their occurrence is also much more blurred.

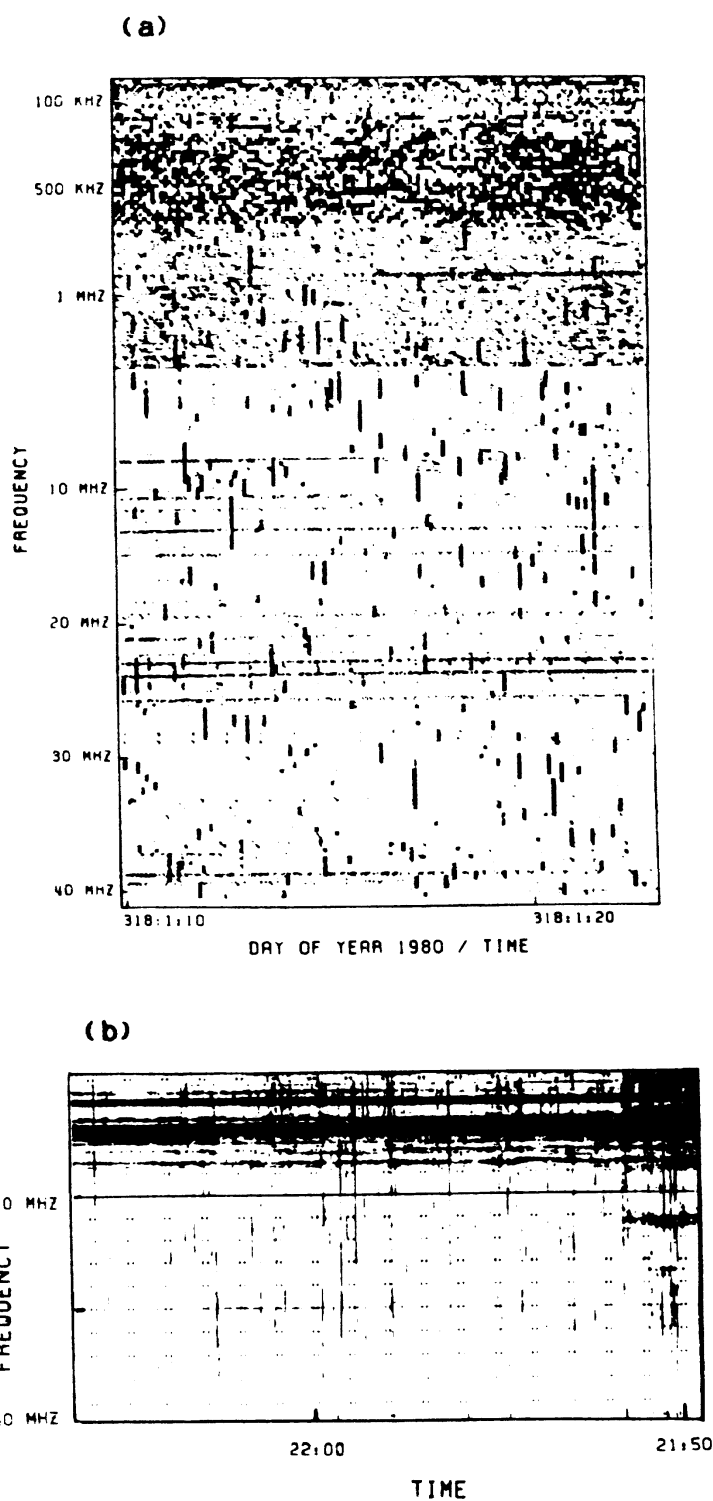


Figure 2: (a) Dynamic spectrum of SED obtained by the V1 PRA experiment about 1 hour after closest approach (from Zarka, 1985a). (b) Dynamic spectrum of radio discharges associated to terrestrial lightning recorded with the decameter array, at Nancay (France). The horizontal dark lines are interference.

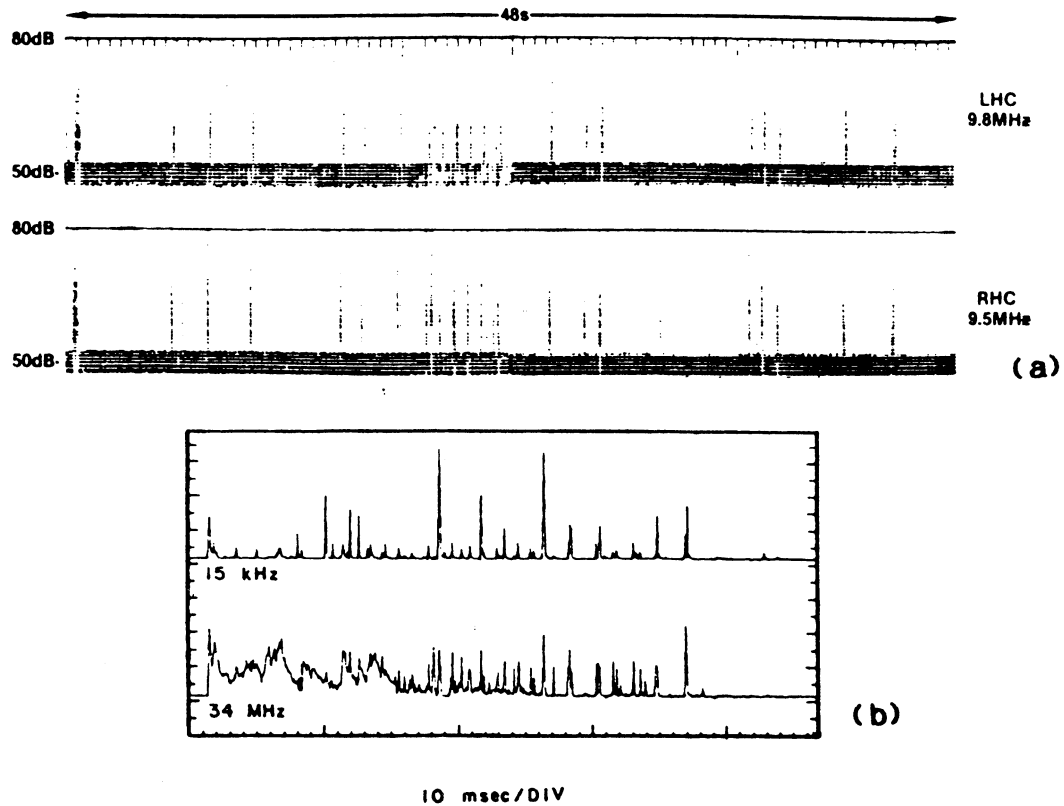


Figure 3: (a) High-time resolution measurements of SED at 9.5 and 9.8 MHz in right- and left-hand circular polarization (from Warwick et al., 1981). (b) High-time resolution radio signature of terrestrial lightning at high (34 MHz) and low (15 kHz) frequencies (from Warwick et al., 1979).

The SED episode centered on V1 closest approach is wider than the other ones. This can be explained by the fact that the phase of the repetition period has been found to be fixed relative to the line between the planet and the spacecraft, implying that the SED source revolves around Saturn like a searchlight and is not fixed relative to the sun, as is the case for SKR [Warwick et al., 1982]. The encounter episode being the only one for which the spacecraft motion matches the rotation of the source, the time during which the SED source stays within sight of the PRA antennas is longer than for the other episodes.

A careful analysis of the episode periodicity has allowed Zarka and Pedersen [1983] to show that the repetition period was slightly smaller for the V2 encounter (10h 00min) than for the V1 encounter (10h 09min). Additionally, some puzzling features first reported by Evans et al. [1981] and Kaiser et al. [1983] appear on Figure 5.

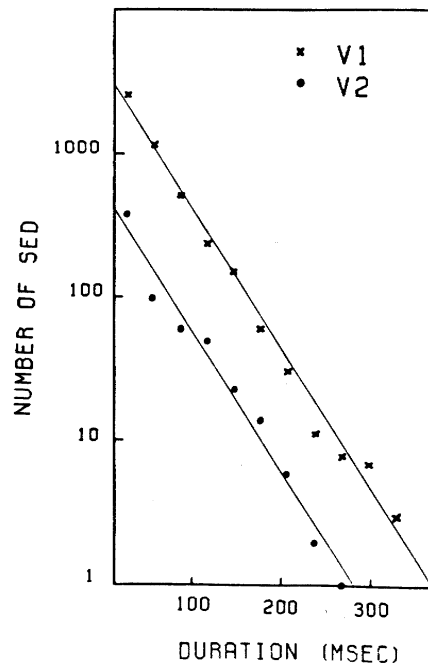


Figure 4: Distributions of SED durations as recorded by V1 and V2 during ~ 6 hours around each encounter (from Zarka, 1984).

- a) As well for V1 as for V2, almost no burst was detected below 6 MHz before closest approach (i.e. from the daylit hemisphere of Saturn) while they appear down to the PRA low frequency band after closest approach (see Figure 2a).
- b) While the onset of all episodes but one is approximately independent of frequency, SED appeared at high frequencies at the beginning of the episode centered on V1 closest approach, and progressively filled the entire PRA band over a 4-hr interval. During this time the occurrence rate of SED in the 30 to 40 MHz band increased from ~ 0.04 per second to the maximum rate of ~ 0.2 per second.
- c) On Figure 5c SED stay visible during a longer time after V1 closest approach than before.
- d) During a typical SED episode the number of observed bursts increases from almost zero to a maximum, and then declines until disappearance. However, before V1 encounter, the episodes exhibit a more complex shape with a small “hump” followed by a higher one.

3.3 Spectrum

Evans et al. [1981] suggested from burst countings that the SED spectrum was “flat” in the range 0.1 - 40 MHz. Zarka and Pedersen [1983] computed the true SED power spectrum, taking into account the response curve versus frequency of the PRA receiver [Ortega-Molina and Daigne, 1984] and its absolute calibration. This spectrum is reproduced on Figure 6 in the validity range of the response curve calculations, i.e. 1–26 MHz.

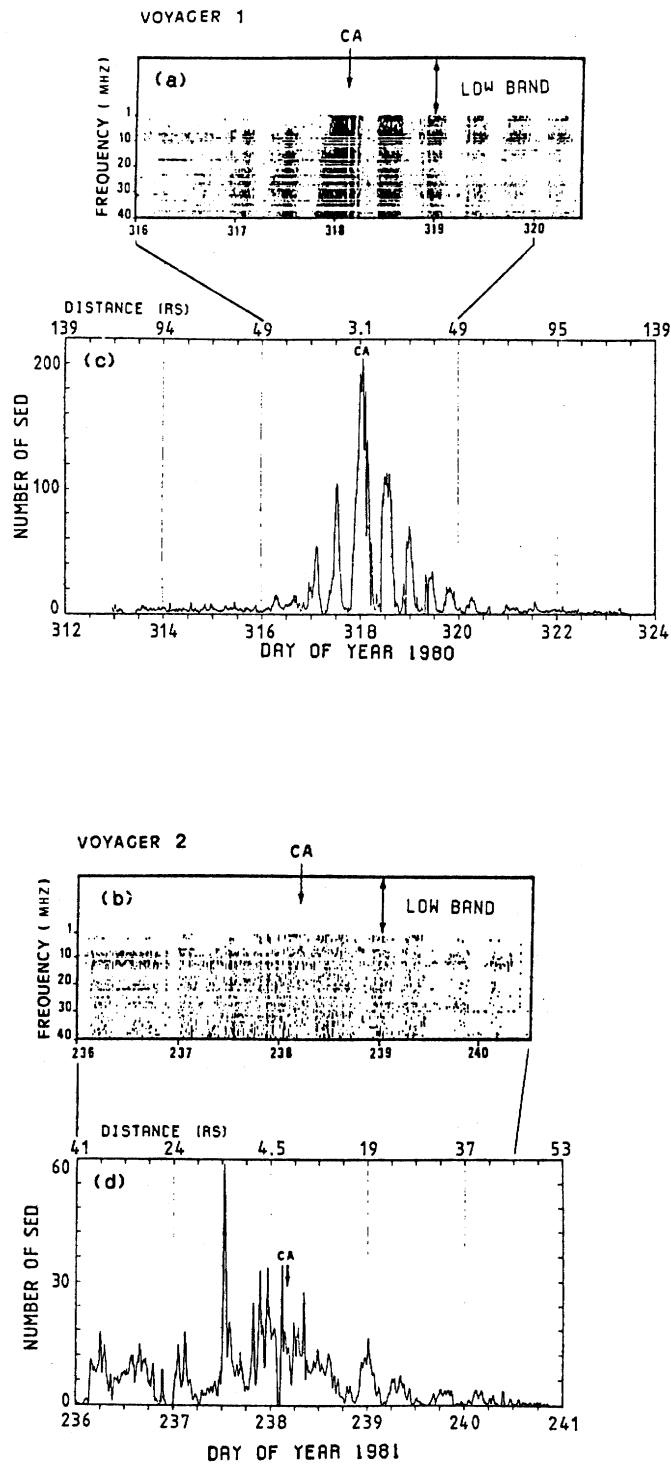


Figure 5: The upper panels (a,b) display SED events detected in the PRA high-frequency band with a compressed time scale. The lower panels (c,d) show overall occurrence of SED for V1 and V2 encounters. CA means closest approach to Saturn (adapted from Zarka and Pedersen, 1983).

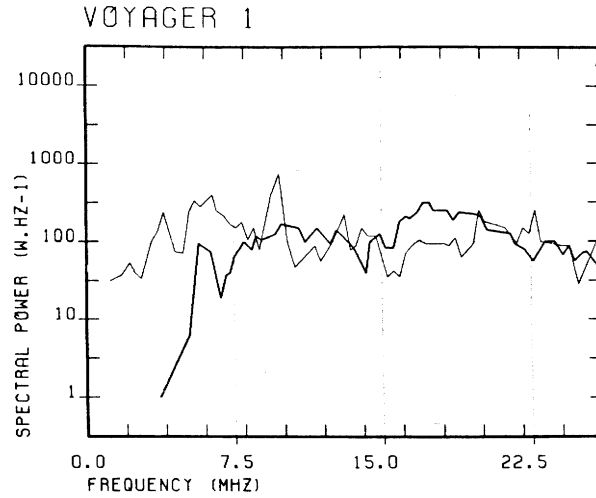


Figure 6: SED power spectrum in the range 1–26 MHz. The error bars associated with the plotted values are about ± 5 dB. The low-frequency cutoff at 6 MHz is visible on the spectrum computed from V1 pre-encounter data (solid line). The spectrum computed from post-encounter data (lightface line) is nearly flat over the range 1–26 MHz (from Zarka and Pedersen, 1983).

Zarka and Pedersen [1983] also showed that SED could appear down to 20 kHz after closest approach. A spectral power of ~ 100 W Hz $^{-1}$ over a 40 MHz bandwidth corresponds to an average SED power of 4×10^9 W ($> 10^{10}$ W for the most intense bursts) and to a flux density about 400 Jy at the orbit of the Earth. However, an earth-based attempt to detect SED at 21 cm (1420 MHz) during V2 fly-by [Lecacheux and Biraud, 1982] and subsequent attempts at frequencies between 40 and 1420 MHz gave negative results. This implies an upper limit of a few Jy on the flux density of SED at frequencies about 1000 MHz, and indicates consequently a spectrum steeper than f^{-1} (and probably of the order of f^{-2}) above 40 MHz. A composite SED spectrum summarizing the results is displayed on Figure 7.

3.4 Polarization

As well on dynamic spectra (Fig. 2a) as on high rate data (Fig. 3a), most SED bursts appear unpolarized. However, Evans et al. [1981] deduced from statistics of the number of SED detected in left- and right-hand channels that after V1 encounter, 90 % of the bursts detected above 15 MHz were left-hand polarized. However, Zarka and Pedersen [1983] showed that these results were subject to very large uncertainties (35 to 100 %) and strongly dependent on instrumental and geometrical factors. Zarka [1984] defined a polarization index for the channel (i):

$$P(i) = \frac{\langle I_L(i) \rangle - \langle I_R(i) \rangle}{\langle I_L(i) \rangle + \langle I_R(i) \rangle}$$

where $\langle I_L(i) \rangle$ (resp. $\langle I_R(i) \rangle$) represents the average intensity measured in left-hand (resp. right-hand) polarization in channel (i), and showed that the SED emission was globally unpolarized (as shown on Figure 8).

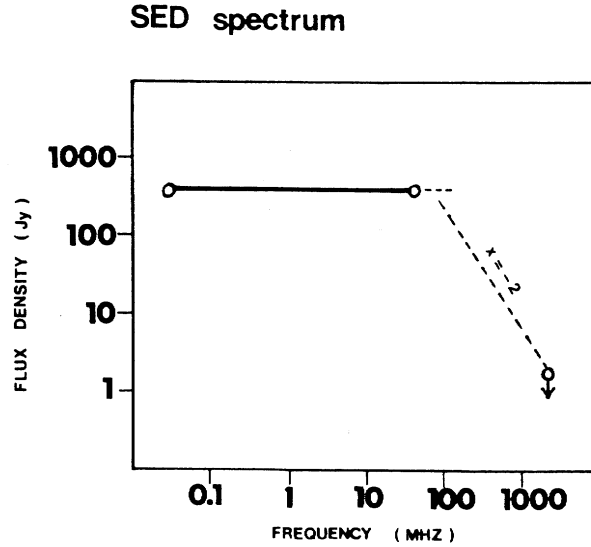


Figure 7: Composite SED spectrum. The low-frequency part (20 kHz – 40 MHz) is given by Voyager PRA observations. The high-frequency part is an upper limit constrained by earth-based experiments (adapted from Lecacheux and Biraud, 1982).

Only a few percent of the bursts appear polarized, with a roughly equal number of left- and right-hand circular polarization. This polarization is probably due to propagation, a discharge being expected to be unpolarized.

3.5 Conclusion

While the intrinsic characteristics of SED (duration, spectrum, polarization) did not change between the two Voyager–Saturn encounters, the global characteristics of the emission (number of bursts, periodicity of occurrence and short time-scale fluctuations) have changed in 9 months. This proves that the SED source strongly evolves with time.

4 Source location

Only two source locations were deemed possible due to the value of the repetition period of the SED occurrence: inside the B-ring at $\sim 1.8 R_S$ ($R_S =$ Saturn radius) where the Keplerian revolution period equals 10h 09min, or within the equatorial atmosphere where the cloud top wind velocities (displayed on Figure 9) added to Saturn’s rotation correspond to a period about 10h 10min.

From the statistical results above, Burns et al. [1983] and Kaiser et al. [1983] inferred that the SED source must be located in Saturn’s equatorial atmosphere. This interpretation allows to account for most of the observed SED characteristics. The major argument of Kaiser et al. [1983] is that the on-off pattern of SED episodes corresponds better to the occultation pattern of a 60° -wide atmospheric source than to those of a ring-source at

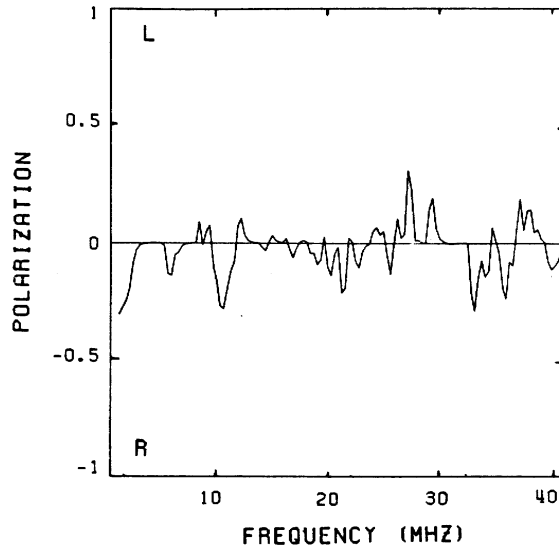


Figure 8: Polarization as a function of frequency for a typical SED episode (V1–Saturn encounter). The polarization index is defined in the text. A three–point running mean has been used to smooth the curve. Only SED covering at least two PRA channels have been taken into account, in order to reduce the statistical errors (adapted from Zarka, 1984).

1.8 R_S , or an atmospheric point source, as displayed on Figure 10 (the emission being assumed isotropic in all cases).

Moreover, the variation of the SED low–frequency cutoff from before to after encounter can be explained by strong diurnal variations of the equatorial ionospheric peak electron density. A dayside value of $N_e = 4 \times 10^5 \text{ cm}^{-3}$ prevents the escape of atmospheric radio bursts below 6 MHz, according to the formula:

$$f_p(\text{kHz}) = 9\sqrt{N_e(\text{cm}^{-3})}$$

where f_p is the plasma frequency, while there should be very low density regions or holes in the nightside ionosphere ($N_e = 5\text{--}100 \text{ cm}^{-3}$) in order to allow the detection of SED at frequencies as low as 20–100 kHz. The frequency dependence of the onset of the SED episode centered on V1 closest approach can then be explained by the fact that the cutoff frequency (f_c) for a wave with an angle of incidence (Θ) at the ionosphere writes:

$$f_c = \frac{9\sqrt{N_e}}{\cos \Theta}$$

At each reappearance of the SED source, Θ decreases progressively from 90° to 0° as the SED source moves from the limb of the planet to the center of the disk. The cutoff frequency (f_c) therefore sweeps the PRA range from 40 MHz to f_p . The symmetrical phenomenon occurs at each disappearance of the SED source. However, for a fixed observer, a typical reappearance or disappearance takes only a few minutes, a periodicity of 10h

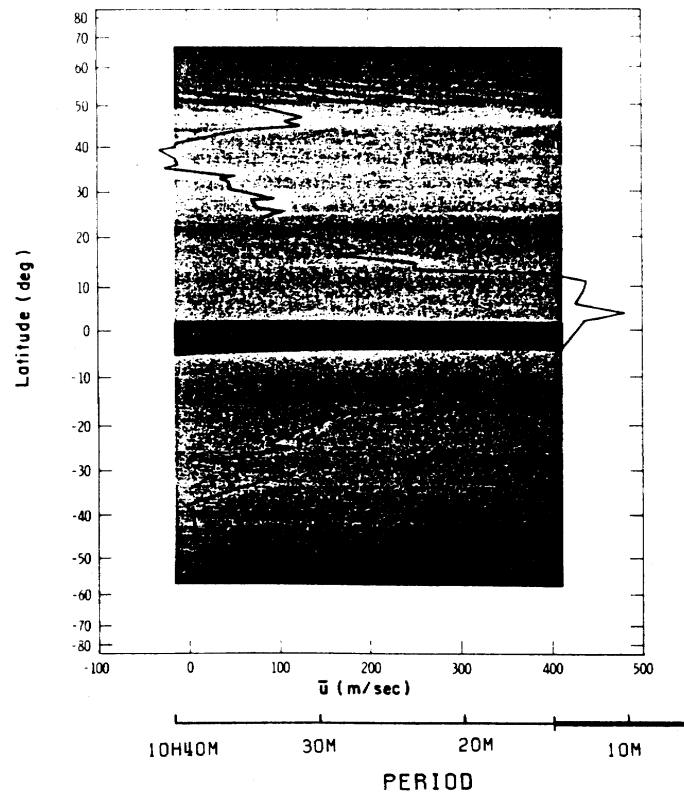


Figure 9: Profile of Saturn mean cloud top wind velocities, measured relative to the radio period of 10h 39.4min, and associated rotation period, overlaid on a cylindrically projected image of Saturn. The dark equatorial band is produced by the shadow of the rings. The winds flowing eastward, the clouds super-rotate relative to the planet (adapted from Smith et al., 1981 and Burns et al., 1983).

10min corresponding to a drift rate of $\pm 1.5 \text{ MHz min}^{-1}$. Such a large drift rate is not discernible in the SED data due to the sparsity of SED near the edges of the episodes. But, at the beginning of the episode centered on V1 closest approach, the spacecraft was no more a fixed observer relative to Saturn. During a few hours, its motion nearly matched the planetary rotation. Consequently, the time scale is considerably expanded for the first half of the V1 encounter episode, and the corresponding onset drift rate is only 0.2 MHz min^{-1} , which is perfectly discernible and leads to a rise time about 4 hours for the SED source, as observed on Figure 5a. At the end of this episode, V1 was no longer corotating with Saturn, so the source disappeared quickly, over the drawn meridian. Additionally, the growth of the SED occurrence rate during these 4 hours (see 3. 2.b) would be due to the increase of the visible part of the 60° -wide SED source during its reappearance.

These results are strongly in favour of an atmospheric storm system as the source of SED. However, is the ring source concept definitely eliminated?

The ring location was the first retained by Warwick et al. [1981, 1982] due to the fact that SED were sometimes observed at frequencies well below the plasma frequency ($\sim 1 \text{ MHz}$) measured at the limb of the planet by the Radio Science experiment [Tyler et

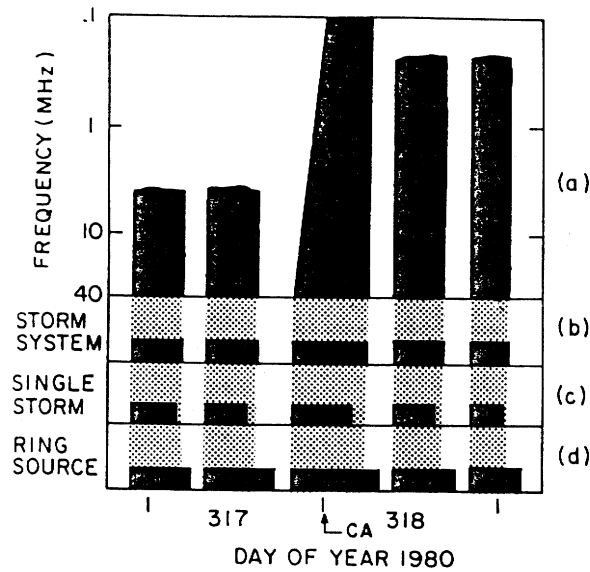


Figure 10: Comparison of observed and predicted recurrence patterns for the five SED episodes centered on V1 closest approach (CA). Panel (a) is a schematic representation of Figure 5a. Panels (b), (c) and (d) display the predicted recurrence patterns for a 60° -wide atmospheric storm system, a single-point atmospheric storm and a single-point source in the B-ring at $1.8 R_S$, respectively. The emission is assumed isotropic in all cases. The agreement is better for a 60° -wide atmospheric source (from Kaiser et al., 1984b).

al., 1981, 1982]. However, Kaiser et al. [1983] showed that these bursts were observed only from the nightside of the planet, as noted above, and thus eliminated this argument against an atmospheric source of SED.

Later, Evans et al. [1982, 1983] found in the V2 photopolarimeter data an isolated 150-m gap in the B-ring at $\sim 1.81 R_S$, and identified a very narrow feature in the same vicinity on a Voyager high-resolution (~ 5 km) image. But, as noted by Burns et al. [1983], no such narrow gap appears in the signal received by the UV spectrometer during the same occultation, and the Voyager high-resolution images are full of narrow features at the resolution limit. Moreover, as it is written above, the SED periodicity at the time of V2 encounter was about 10h 00min and would correspond to a source location at $1.78 R_S$ in the B-ring.

It remains that puzzling observed SED features were still unexplained (see 3. 2.c, d), and that one could argue that a non-isotropic (and, why not, chromatic) ring source could fit the SED occultation pattern and explain the frequency dependent features. The study of the directivity of the SED emission and its ionospheric implications [Zarka, 1985a] will allow us to definitely settle and eliminate the ring location for the SED source.

5 Directivity of SED

Figure 11 displays the distribution of SED intensities as a function of time for the main part of V1 encounter. The flux density corresponding to each SED event detected in the high frequency band of the PRA receiver (1.2 - 40.2 SHz) is plotted versus time, after being corrected for instrumental effects. The threshold at $\sim 3 \times 10^{-19} \text{ W m}^{-2} \text{ Hz}^{-1}$ corresponds to the detection limit of SED above the background due to cosmic radio noise and spacecraft interference. The envelope of the distribution, i.e. the peak SED intensity as a function of time, is also plotted on Figure 11 (for the detailed obtainment of this envelope, see Zarka [1985a]).

This envelope is reproduced on Figure 12, together with a model of the SED intensity which would be received by the V1 PRA experiment from an isotropic equatorial atmospheric source of width L , revolving around Saturn in 10h 09min and occulted by the planet at each revolution. The 0 dB level has been fixed to the SED detection threshold. Figure 12 displays the best fit of the model to the observations, for which $L = 64^\circ \pm 9^\circ$ and the median point of the source is at local time $18\text{h } 40\text{min} \pm 16\text{min}$ at closest approach. These values are consistent with those found by Kaiser et al. [1983].

On Figure 12 the agreement between the two curves is very good after encounter (except at the edges of the episodes) while there are systematic differences between the measured and calculated values of the SED maximum intensity before encounter. Pre-encounter episodes appear “double-humped” as in the SED occurrence diagrams (see 3. 2.d and Figure 5c). Moreover, even for the higher hump, the observed intensities are slightly lower than expected (1–3 dB, depending on frequency). Zarka [1985a] showed that this change in the envelope shape of episodes between pre- and post-encounter could only be due to the propagation of the waves through the sub-spacecraft Saturnian ionosphere, whose parameters are the only ones to have significantly changed from before (dayside) to after (nightside) closest approach.

As we have seen above, SED were detected well below 6 MHz, and sometimes down to 20–100 kHz after V1 closest approach. This implies a low electron density in Saturn’s nightside ionosphere (of the order of 10^3 cm^{-3} according to Kaiser et al. [1984a]). The corresponding plasma frequency f_p is about 300 kHz. Consequently, most SED occurring after closest approach in the high-band of the PRA receiver (1.2 - 40.2 MHz) appear at frequencies $\gg f_p$, and are thus unaffected by their propagation to the spacecraft through the nightside ionosphere of Saturn. So from the post-encounter part of Figure 12, one can deduce the beaming pattern of the SED emission, which is the only parameter not taken into account in the model.

Figure 13 displays the total emission lobe of the SED source. On this figure, the difference between the measured and calculated intensities is plotted in polar coordinates (centered on the median point of the source (M) and relative to the direction Saturn–source (Θ) for the three post-encounter episodes. This emission lobe is quasi-isotropic in the half-space crossed by V1, except for the values of $\Theta \geq 70^\circ$, which correspond to the disappearances of the SED source. Such a result is consistent with the burstiness of the emission – an electrostatic discharge is expected to have a wide beaming pattern –, and with the isotropy

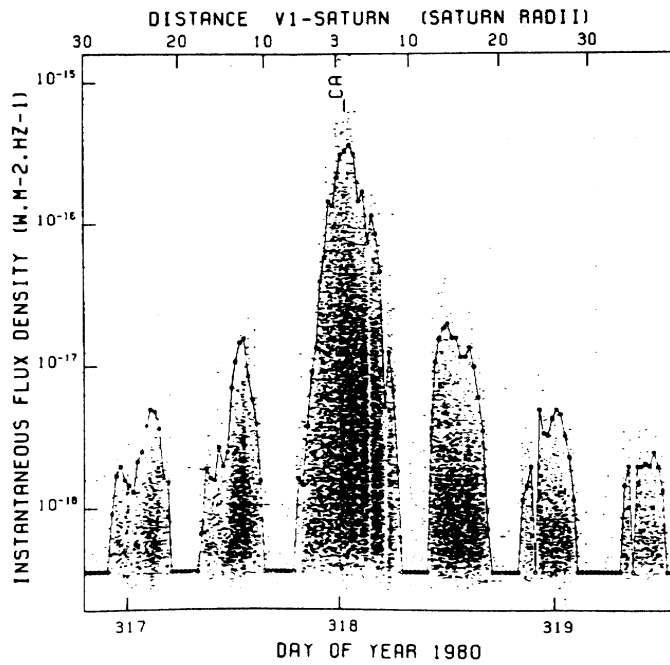


Figure 11: Distribution of SED intensities versus time and distance to Saturn, corrected for instrumental effects. CA indicates V1 closest approach to Saturn. There is a data-gap in each of the last two episodes (from Zarka, 1985a).

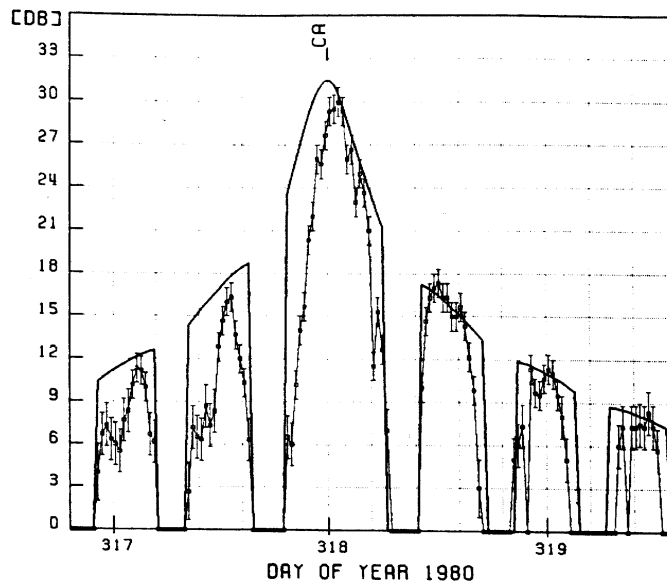


Figure 12: Best least-squares fit of the experimental and calculated variations with time of SED maximum intensity (from Zarka, 1985a).

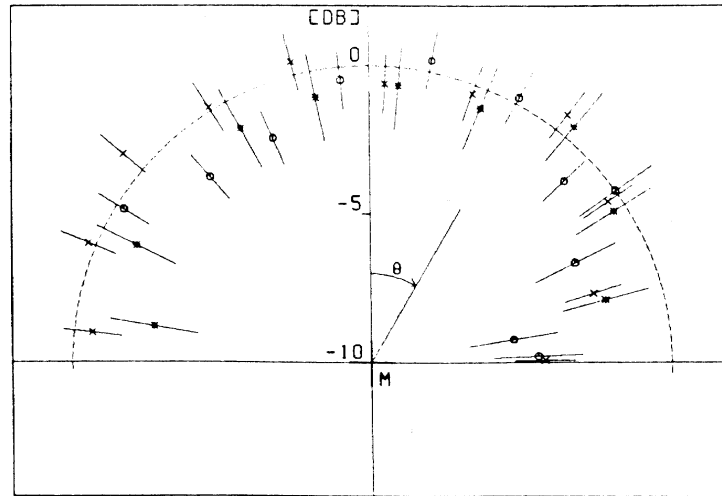


Figure 13: Emission lobe of the SED source derived from the 3 post-encounter episodes. The symbols used are, respectively, x , o and $*$ for the first, second and third post-encounter episode. The dashed curve indicates an isotropic beaming pattern. M and Θ are the median point of the source and the angle between the direction of V1 as seen from the source and then perpendicular to the source motion (from Zarka, 1985a).

of terrestrial lightning radio emission, always assumed in the literature. The particular case of $\Theta \geq 70^\circ$ will be discussed later on.

6 Ionospheric implications

With an isotropic SED emission, the shape of pre-encounter episodes can now be understood in terms of ionospheric propagation. Radio waves propagating through Saturn's ionosphere may suffer refraction (or reflection) and absorption. As Figure 11 includes SED appearing between 1 and 40 MHz, and since the SED spectrum is flat over this frequency range, the shape of pre-encounter episodes cannot be due to a cutoff effect but certainly results from an absorption effect, which is the only one to affect the intensity of the detected bursts. This implies strong variations of the dayside peak electron density with local time.

Quantitative results have been obtained from the study of the detailed variations of the SED low-frequency cutoff before encounter. Figure 14 displays the variations of this cutoff frequency f_c observed during the episode before closest approach, as a function of the local time angle of the SED source. The very high values of f_c (~ 15 MHz) at the edges of the episode are due to the fact that the source is at the limb of the planet, as seen from V1 ($\Theta \sim 90^\circ$).

The variations of the dayside electron density N_e displayed on Figure 15 are deduced from the cutoff frequencies f_c of Figure 14 according to the expression:

$$N_e(\text{cm}^{-3}) = [f_c(\text{kHz}) \cdot \cos \Theta]^2 / 81.$$

On Figure 15 are also plotted the peak electron densities measured by the Radio Science experiment on V1 and V2 [Tyler et al., 1981, 1982] and the values deduced by Kaiser et al. [1984] from a similar study of the SED low-frequency cutoff through a ray-tracing analysis. These results are complementary and give a complete coverage in local time for the variations of N_e . In spite of the large uncertainties due to the wide longitudinal extent of the SED source, two regions can be distinguished in the dayside ionosphere: a morning region from LT \sim 9h 30min to 14h where the mean electron density is $\sim 6 \times 10^5 \text{ cm}^{-3}$ and an evening region from LT \sim 16h to 18h where the mean electron density is about $3.5 \times 10^5 \text{ cm}^{-3}$.

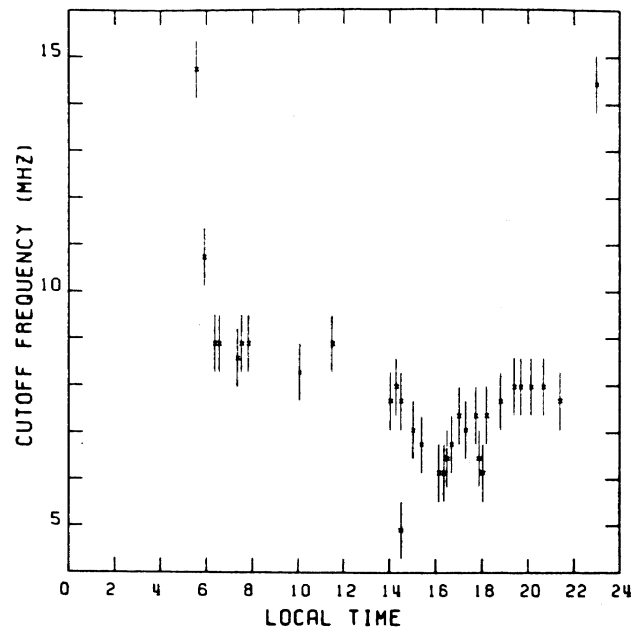


Figure 14: Measured SED low-frequency cutoff as a function of the local time angle of the SED source for the episode before V1 closest approach. The error bars represent $\pm 300 \text{ kHz}$, which correspond to the frequency gap between two adjacent channels in the high-frequency band of the PRA receiver (from Zarka, 1985a).

The absorption curves computed between 8 and 40 MHz (above cutoff frequencies) with these values of the electron density are plotted on Figure 16, together with the SED spectra obtained during the two halves of the episode before closest approach and corresponding to the scanning by the SED source of the two regions of the dayside saturnian ionosphere defined above. For the detailed calculations of the absorption (non-deviative, resulting from the collisions of electrons with ions), see Zarka [1985a]. These spectra are very noisy due to the small number of bursts involved in the analysis, but their global agreement with the computed absorption curves is good, especially for the low-frequency part of the diagram ($f \leq 20 \text{ MHz}$) where the effect of the absorption is important.

This agreement confirms the values of Figure 15 for the dayside equatorial ionosphere, and explains the envelope shape of pre-encounter episodes, which is due to stronger absorption of SED through the morning side of the ionosphere at the beginning of these episodes. Due to the presence of a fixed detection threshold for the PRA receiver, the smaller number

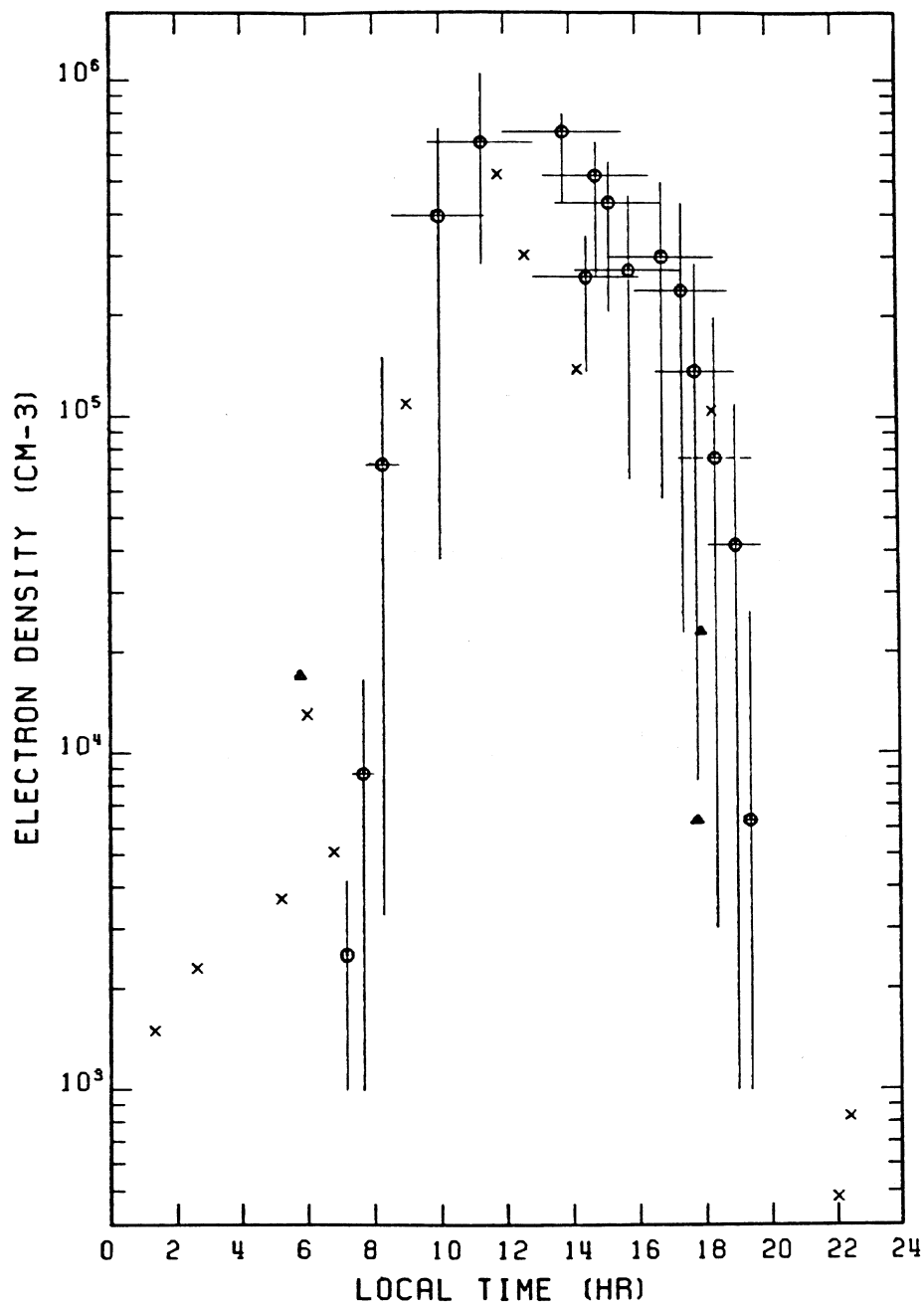


Figure 15: Diurnal variations of the peak electron density in the dayside equatorial ionosphere of Saturn, deduced from Figure 14. Ordinate error bars represent the range of electron densities which can account for the observed cutoff frequency, given the longitudinal extent of the SED source visible from V1 at the time of the measurement (abscissa error bars). They also include the uncertainty on the cutoff frequency quoted on Figure 14, although almost negligible. In the case for which two or more points deduced from the values of Figure 14 had very close coordinates and error bars, only the mean point has been plotted. The values deduced by Kaiser et al. [1984a] from a ray-tracing analysis of the PRA data are also plotted on the figure (as "x", the corresponding error bars, similar to ours, being omitted for clarity), together with the peak electron densities measured by the Radio Science experiments [Tyler et al., 1981, 1982] (Δ), (adapted from Zarka, 1985a, and Kaiser et al., 1984a).

of SED bursts detected at the beginning of these episodes is also explained by the same absorption effect, which reduces the intensity of most low-frequency ($\leq 15\text{--}20$ MHz) SED events below the detection threshold.

The longer extent of the SED visibility after V1 closest approach can be explained by the fact that after encounter, SED no more suffer absorption as they propagate through Saturn's nightside ionosphere, and consequently they are globally observed 1–3 dB more intense than before encounter, so that they remain a longer time above the PRA detection threshold.

Finally, the discrepancy between the SED beaming pattern and a true isotropic one for $\Theta \geq 70^\circ$ is only due to the fact that after closest approach, the SED source disappears under the morning side ionosphere at the end of each episode. Here again, absorption due to the high electron density in this region of the ionosphere explains the reduction of the observed SED intensity on the right part of the emission lobe of Figure 13. The total beaming pattern of SED is therefore isotropic.

Although qualitatively in agreement with most of the results above, no quantitative result has been obtained from V2 PRA data, principally due to the very fluctuating occurrence rate of SED and to their blurred episode structure for the V2 encounter.

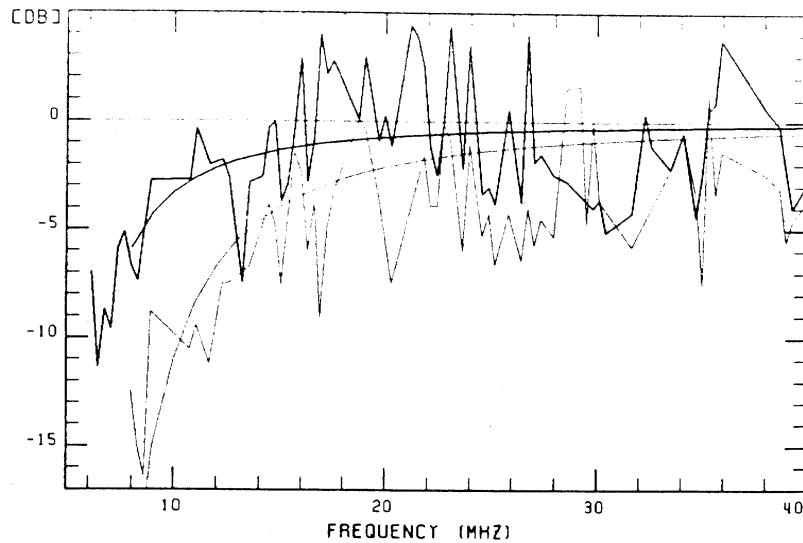


Figure 16: The broken lines display as a function of frequency the maximum SED intensity detected during the first half (day 317, 7h to 11h, lightface line) and the second half (day 317, 11h to 15h, solid line) of the episode before V1 closest approach. Due to the small number of events appearing in each channel, error bars about ± 5 dB are associated with the quoted values. The smooth lines are absorption curves computed for values of the electron density of $3.5 \times 10^5 \text{ cm}^{-3}$ (solid line) and $6 \times 10^5 \text{ cm}^{-3}$ (lightface line). (from Zarka, 1985a).

7 Conclusions

Table 1 summarizes all the results obtained about SED, and their interpretation in terms of an atmospheric or a ring source. For the case of the atmospheric source, the character-

istics of SED are compared with those of other planetary lightning. We must note that in the case of Earth, most data is concerned with cloud to ground lightning strokes, whereas SED have to be compared to cloud-to-cloud strokes. However, while nearly all SED characteristics can be well explained in the case of an atmospheric source, only a few of them receive an explanation with a ring source. Moreover, the problem with this latter interpretation is not only that many questions remain unanswered, but principally that some of the conditions (noted *) required for explanation of the observed SED characteristics are totally incompatible together.

So, we definitely eliminate the ring source interpretation and conclude that the SED source lies in Saturn's equatorial atmosphere. The simplest explanation, given by Kaiser et al. [1983] is then a 60°-wide storm system, SED being the Saturnian lightning associated radio emission.

The important changes of SED characteristics from V1 to V2 encounter must then be attributed to variations at the source, as the structure of Saturn's ionosphere did not change dramatically in the 9 months separating the two encounters [Tyler et al., 1981, 1982]. So, either V1 and V2 observed two different storm systems, which would imply a lifetime longer than about a week (one encounter period) but shorter than 9 months for a given storm system, or it is the same storm system which has been observed by both spacecraft. In that case, the observed differences would imply a longitudinal spreading of the source region in 9 months, due to the fluctuations of the equatorial wind velocities with time and latitude, and a weakening of its emission. The discreteness of SED episodes for the V1 encounter could then suggest that the observed storm system was not formed a long time before the first Saturn encounter.

The last remaining serious problem with this lightning interpretation of SED was (as noted by Burns et al. [1983] and Kaiser et al. [1984b]) the lack of detection of SED-like bursts from Jupiter and the Earth, although these planets do have a strong lightning activity. However, Zarka [1985b] recently showed that for the Earth and Jupiter, strong absorption occurs in the lower layers of the ionosphere due to collisions of electrons with neutral particles, and prevents the escape of SED-like radio bursts from these planets. This indicates indirectly the absence of low-altitude ionospheric layers with a high electron density on Saturn.

We also note that if the large variations of Saturn's ionospheric peak electron density between day and night are comparable to those of the E and F1 layers of the terrestrial ionosphere [Davis, 1965], the observed morning side maximum is unusual for planetary ionospheres. It might be due to an ionization source different from the solar EUV radiation.

8 The future

As we have seen in section 3.3, a spectral power of 100 W Hz⁻¹ corresponds to a flux density about 400 Jy at the Earth (in the range 1–40 MHz). Consequently, ground-based radiotelescopes suitably equipped should be able to detect SED.

OBSERVED PROPERTY OF SED	ATMOSPHERIC SOURCE	RING SOURCE
Periodicity $\sim 10\text{h}10\text{min}$ ($\sim 10\text{h}00\text{min}$ for V2)	Cloud tops at equator	Keplerian period at $\sim 1.8 R_S$
Distinct episodes	Occultation pattern	Directive beaming pattern necessary (*)
Variable occurrence rate within episodes	Multiple storm cells?	Ring particles collisions?
Inter-episodes events	Isolated storms?	?
Poisson distribution of the SED occurrence per time unit	Lightning discharges	Ring particles collisions?
SED duration: 30–450 ms (elementary < 1 ms)	Comparable to terrestrial and other planetary lightning (elementary ~ 1 ms for the Earth)	?
Exponential distribution of durations: $D_0=45$ ms, mean= 57 ms	Log-normal for the Earth, mean=34 ms	?
Size of the instantaneous radio source ≤ 40 km	Cloud-to-cloud lightning	Ring particles collisions
Broadband spectrum, \sim flat in the range 20 kHz – 40 MHz and steeper than f^{-2} above 40 MHz	Lightning broadband spectrum. For the Earth, decreases in f^{-2} above ~ 100 kHz	Broadband spectrum of a discharge in the free-space (*)
SED usually unpolarized	Lightning	Discharges
Low-frequency cutoff after closest approach: $\sim 20\text{--}100$ kHz	Low-density regions or holes in Saturn's nightside ionosphere	No highly ionized ring plasma
Low-frequency cutoff before closest approach: 6 MHz	High electron density in the dayside ionosphere	?
Frequency drift of the onset of the V1 encounter episode	Thunderstorm rising over the limb	Chromatic emission lobe ? (*)
Longer visibility of SED after closest approach	Greater ionospheric absorption through the dayside than through the nightside ionosphere	?
“Double-humped” episodes before closest approach	Diurnal variations of the ionospheric dayside peak electron density	?
Beaming pattern	Isotropic (as terrestrial lightning?)	Isotropic for an electrostatic discharge in the freespace (*)
Total power $\sim 10^9$ W (10^7 to 10^{10} W)	Higher than other planetary lightning	?

Table 1: SED properties and source location (adapted from Burns et al., 1983, and Zarka, 1984). (*) indicates incompatible conditions.

The attempt will be made soon at Nancay with an Acousto-optical-spectrograph (SAO) coupled to the decameter array. The SAO is a broadband spectrograph (20 MHz bandwidth) with a time resolution about 50–100 ms. The minimum detectable flux is ≤ 100 Jy. So, except if SED activity has dramatically decreased since the V2–Saturn encounter, they will be detectable from Nancay.

In the other case, we will have to wait until the V2–Uranus encounter in January 1986 with the hope to detect UED (Uranus electrostatic discharges) in order to learn more about planetary lightning, atmospheres and ionospheres.

9 References

- Burns, J. A., M. R. Shoewalter, J. N. Cuzzi, and R. H. Durisen, Saturn electrostatic discharges: Could lightning be the cause?, *Icarus*, **54**, 280, 1983.
- Davies, K., Ionospheric radio propagation, *NBS Mono.*, 80, Washington, 1965.
- Evans, D. R., J. W. Warwick, J. B. Pearce, T. D. Carr, and J. J. Schauble, Impulsive radio discharges near Saturn, *Nature*, **292**, 716, 1981.
- Evans, D. R., J. H. Romig, C. W. Hord, K. E. Simmons, J. W. Warwick, and A. L. Lane, The source of Saturn electrostatic discharges, *Nature*, **299**, 236, 1982.
- Evans, D. R., J. H. Romig, and J. W. Warwick, Saturn's electrostatic discharges: Properties and theoretical considerations, *Icarus*, **54**, 267, 1983.
- Kaiser, M. L., J. E. P. Connerney, and M. D. Desch, Atmospheric storm explanation of Saturnian electrostatic discharges, *Nature*, **303**, 50, 1983.
- Kaiser, M. L., M. D. Desch, and J. E. P. Connerney, Saturn's ionosphere: Inferred electron densities, *J. Geophys. Res.*, **89**, 2371, 1984a.
- Kaiser, M. L., M. D. Desch, W. S. Kurth, A. Lecacheux, F. Genova, B. M. Pedersen, and D.R. Evans, Saturn as a Radio Source, in *Saturn*, edited by Gehrels T. and Matthews M. S., 378, The University of Arizona Press, 1984b.
- Lecacheux, A. and F. Biraud, An Earth-based attempt to detect SED at 21 centimeters, in *Proceedings of the IAU Colloquium 75: Planetary rings*, Toulouse, 1982.
- Ortega-Molina, A. and G. Daigne, Polarization response of two crossed monopoles on a spacecraft, *Astron. Astrophys.*, **130**, 301, 1984.
- Smith, B. A. and 26 co-authors, Encounter with Saturn: Voyager 1 imaging science results, *Science*, **212**, 163, 1981.
- Tyler, G. L., V. R. Eshleman, J. D. Anderson, G. S. Levy, G. F. Lindal, G. E. Wood, and T. A. Croft, Radio science investigations of the Saturn system with Voyager 1: Preliminary results, *Science*, **212**, 201, 1981.
- Tyler, G. L., V. R. Eshleman, J. D. Anderson, G. S. Levy, G. F. Lindal, G. E. Wood, and T. A. Croft, Radio science with Voyager 2 at Saturn: Atmosphere and ionosphere and the masses of Mimas, Tethys and Iapetus, *Science*, **215**, 553, 1982.

- Warwick, J. W., J. B. Pearce, R. G. Peltzer, and A. C. Riddle, Planetary radio experiment for the Voyager missions, *Space Sci. Rev.*, **21**, 309, 1977.
- Warwick, J. W., C. O. Hayenga, and J. W. Brosnahan, Interferometric directions of lightning sources at 34 MHz, *J. Geophys. Res.*, **84**, 2457, 1979.
- Warwick, J. W., J. B. Pearce, D. R. Evans, T. D. Carr, J. J. Schauble, J. R. Alexander, M. L. Raiser, M. D. Desch, B. M. Pedersen, A. Lecacheux, G. Daigne, A. Boischot, and C. H. Barrow, Planetary Radio Astronomy observations from Voyager 1 near Saturn, *Science*, **212**, 239, 1981.
- Warwick, J. W., D. R. Evans, J. H. Romig, J. K. Alexander, M. D. Desch, M. L. Kaiser, M. Aubier, Y. Leblanc, A. Lecacheux, and B. M. Pedersen, Planetary radio astronomy observations from Voyager 2 near Saturn, *Science*, **215**, 582, 1982.
- Zarka, P., Contribution a l'étude des émissions radioélectriques des planètes extérieures, Thèse de 3^{ème} cycle, Paris 6, 1984.
- Zarka, P., Directivity of Saturn Electrostatic Discharges and ionospheric implications, *Icarus*, **61**, 508–520, 1985a.
- Zarka, P., On detection of radio bursts associated with Jovian and Saturnian lightning, *Astron. Astrophys.*, **146**, 15, 1985.
- Zarka, P. and B. M. Pedersen, Statistical study of Saturn electrostatic discharges, *J. Geophys. Res.*, **88**, 9007, 1983.